# Energy & Environmental Science

Accepted Manuscript






ROYAL SOCIETY OF CHEMISTRY

www.rsc.org/ees

Energy & Environmental Science

COMMUNICATION

# High Performance Sulfur-doped Disordered Carbon Anode for Sodium Ion Batteries

Received 00th January 20xx,
Accepted 00th January 20xx

DOI: 10.1039/x0xx00000x

www.rsc.org/

*Wei Li*,[a†] *Min Zhou* [a†], *Haomiao Li*,[a] *Kangli Wang*, *[a] *Shijie Cheng* [a] and *Kai Jiang** [a]

***Sulfur-doped disordered carbon is facilely synthesized and investigated as an anode for sodium ion batteries. Benefiting from the high sulfur doping(~26.9 wt%), it demonstrates a high reversible capacity of 516 mAh $g^{-1}$, excellent rate capability as well as superior cycling stability (271 mAh $g^{-1}$ at 1 A $g^{-1}$ after 1000 cycles)***

Sodium ion batteries (SIBs) are considered as one of the most promising alternative to lithium ion batteries (LIBs) for application in large scale energy storage owning to the abundant natural resources and low environmental impact.[1-6] However, as $Na^+$ is 55% larger than $Li^+$ in radius and the diffusion kinetics of $Na^+$ is much more sluggish, it is difficult to find appropriate host materials with sufficiently large interstitial space to accommodate $Na^+$ and to allow reversible and fast ion insertion/extraction, especially with regard to the anode materials. Up to now, only a few of Na host anode materials have been demonstrated suitable capacity and acceptable cyclability, mainly including carbonaceous materials,[7] metallic alloys, [8-11]and titanates.[12] However, the large volume expansion of metallic alloys during the sodiation and relatively low capacity of titanates severely limit their practical applications.[7] Therefore, numerous researches have been continuously focused on developing novel carbon-based anode materials.

It is well known that graphite, the dominant anode material in commercial LIBs, is not suitable for SIBs, presumably because of the mismatching of graphite interlayer distance ($d_{002}$=0.334 nm) with larger $Na^+$. Disordered carbon appears to be the most suitable anode material for SIBs and various types of non-graphitic carbon materials have been investigated, including MCMB,[13,14] carbon fiber,[15] carbon black,[16] and pyrolyzed carbon.[17] However, their performance is still far from that achieved by graphite in lithium system, with capacity only up to about 250 mAh $g^{-1}$ at very low current density (below 50 mA $g^{-1}$ at the voltage range from 0 to 3V). Recently, many works have been conducted to enhance their capacity and cycling stability by nano-sizing the materials with new structures.[18-28] Significant improvement in reversible capacity was reported by Wan *et al.*, using a sandwich-like hierarchically porous carbon/graphene composite (G@HPC).[28] The G@HPC composite displays a high specific capacity of 400 mAh $g^{-1}$ at 50 mA $g^{-1}$ and long cycling stability (250 mAh $g^{-1}$ at a current rate of 1 A $g^{-1}$ over 1000 cycles).

While exciting progress has been made by designing nanoarchitectures of porous carbon, heteroatom doping (such as N, B, S and P) have been attracting increasing attention, as an effective strategy to tune and enhance the physical and chemical properties of carbon-based materials.[18,21.29-31] Nitrogen is by far the most extensively investigated heteroatom, which could enhance the reactivity and electronic conductivity by generating extrinsic defects.[18,21.29-31] Huang *et al.* firstly reported N-doped carbon nanofibers as anode for SIBs,[29] which delivered a reversible capacity of 73 mA h $g^{-1}$ at the current density of 20 A $g^{-1}$. In comparison to Nitrogen, other heteroatoms doping, such as sulfur and phosphorus, is relatively rare and represents an emerging research field. Sulfur doping is of particular interest for battery applications since sulfur is an electrochemical active element that can reversibly react with Li or

[a] *State Key Laboratory of Advanced Electromagnetic Engineering and Technology, School of Electrical and Electronic Engineering, State Key Laboratory of Materials Processing and Die & Mould Technology, School of Materials Science and Engineering, Huazhong University of Science and Technology, Wuhan 430074, P. R. China. E-mail: kjiang@hust.edu.cn; klwang@hust.edu.cn*
† These authors contributed equally to this work.

Electronic Supplementary Information (ESI) available: Supporting information for this article is given via a link at the end of the document

Na.[32,33] Therefore the introduction of sulfur into the carbon structure may provide additional reaction sites for accommodation of $Li^+$ or $Na^+$, resulting in the increase of specific capacity. Herein, we report for the first time a sulfur-doped disordered carbon, prepared by one step pyrolytic synthesis technique, as the anode material for SIBs. It exhibits a high reversible capacity of 516 mAh $g^{-1}$ at a current density of 0.02 A $g^{-1}$, superior rate capability (158 mAh $g^{-1}$ at 4 A $g^{-1}$) and excellent cyclability (271 mAh $g^{-1}$ after 1000 cycles at 1 A $g^{-1}$ with a capacity retention of 85.9%).

The sulfur-doped disordered carbon (designated as DC-S) was synthesized facilely by annealing the mixture of 1,4,5,8-Naphthalenetetracarboxylic dianhydride (NTCDA) and sulfur in the flowing atmosphere of Ar at 500 °C with an optimized mass ratio of 1:1 for 4 h. Figure 1a shows the illustration of the synthsis of DC-S. For comparison, the pyrolyzed carbon of NTCDA (designated as DC) was prepared by the same method without sulfur. Thermogravimetric analysis (TGA) and Differential thermal analysis (DTA) of the mixture of NTCDA and sulfur (50: 50 wt%) in Ar atmosphere indicate that the carbon sulfurization temperature is at ~340 °C (Figure S1). When the temperature increased to 500 °C, a total carbonization of the NTCDA and carbon sulfurization process is completed, with excess sulfur evaporating off. The elemental analysis (EA) quantifies that the weight contents of C, S, O, H in the DC-S composite are 62.28 wt%, 26.91 wt%, 9.20 wt% and 1.61wt%, respectively (Table S1).

The morphologies of as-prepared DC and DC-S were characterized by field-emission scanning electron microscopy (FESEM) and transmission electron microscopy (TEM), as shown in Figure 1b-e. The DC consists of flake-shaped particles with an average size of 10 um (Figure 1b), while the DC-S sample appears as well-developed 3D coral-like architecture with an average size of 500 nm (Figure 1c). This coral-like 3D structure has many interpenetrative holes leading into large spaces inside the architectures, which is mainly formed by the volatilization of excess sulfur during the sulfurization process. HRTEM image (Figure 1d) reveals the rough surface of the coral-like frameworks with nanopores. Such a hierarchical porous structure can provide a number of interpenetrating channels, allowing the electrolyte to permeate sufficiently into the entire structure and facilitating $Na^+$ transport between the electrode/electrolyte interfaces. EDS elemental mapping (Figure 1e) reveals the homogeneous distribution of carbon, sulfur and oxygen throughout the whole area of the porous carbon.

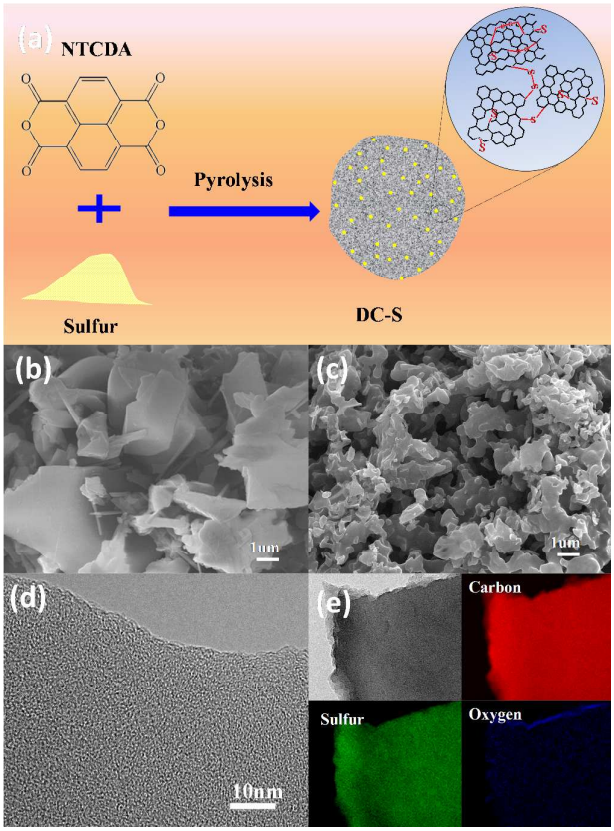


***Figure 1.*** (a) Schematic illustration for preparation of DC-S. SEM image of (b) DC and (c) DC-S; (d) HRTEM image and (e) EDS elemental mapping of DC-S.

Figure 2a compares the XRD patterns of NTCDA, sulfur, DC-S and DC. No diffraction peaks of NTCDA or sulfur are observed in the XRD patterns of DC-S, indicating a total carbonization and sulfurization of NTCDA. The XRD patterns of DC-S and DC show two major broad peaks located at $2\theta$ = 24.6° and 44.8°, corresponding to the (002) and (100) diffraction of disordered carbon structure. According to Bragg's equation, the interlayer spacing of DC and DC-S ($d_{002}$) is calculated to be 3.6159 Å and 3.6598 Å, respectively, indicating both of them are suitable for the intercalation/extracton of $Na^+$.[25] A larger $d_{002}$ value of DC-S compared to the DC implies that sulfur doping can enlarge the interlayer distance of disordered carbon, which may facilitate the diffusion and insertion/extraction of $Na^+$ and increase the electrochemical utilization of disordered carbon. Since the covalent diameter of sulfur is larger than that of carbon, the substitution of carbon by sulfur will cause the increase in the spacing between adjacent sheets. X-ray photoelectron spectroscopy (XPS) was conducted to identify the chemical state of sulfur. The high

resolution S2p spectrum is shown in Figure 2b, which exhibits three peaks at the binding energies of 163.7, 164.8 and 168.4 eV, respectively. The former two dominated peaks can be attributed to the S2p3/2 and the S2p1/2 of the -C-$S_x$-C- ($x$=1-2)covalent bond of the thiophene-S, while the weak peak at 168.4 eV is corresponding to C-$SO_x$-C ($x$=2-4) groups,[34-36] confirming that sulfur has been successfully incorporated into the disordered carbon.

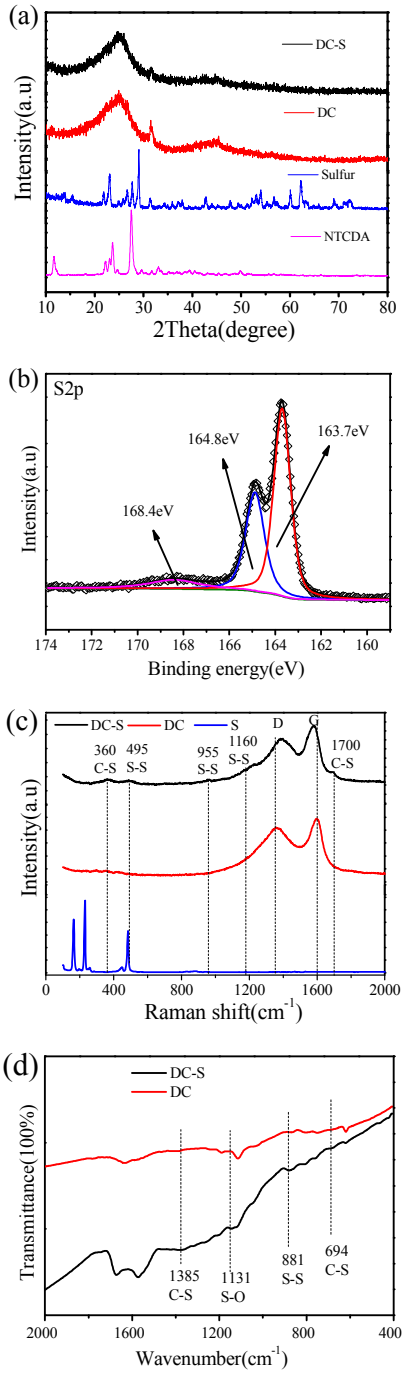


***Figure 2.*** (a)XRD patterns of NTCDA, sulfur, DC and DC-S. (b) XPS spectrum of DC-S. (c)Raman spectra of DC-S, DC and sulphur. (d) FTIR spectra of DC-S and DC.

Further structural information of the DC-S and DC is obtained by Raman and FTIR analysis. Compared to the spectrum of DC, Raman spectrum of DC-S reveals extra distinctive peaks at 360, 495, 955, 1160 and 1700 $cm^{-1}$, shown in Figure 2c. The bands at 1700 and 360 $cm^{-1}$ are assigned to stretch vibration and deformation of C-S bond, and those at 1160, 955 and 495 $cm^{-1}$ are attributed to the stretch vibration of S-S bond,[37,38] indicating that sulfur is atomic bonded to the carbon structure. Furthermore, an obvious upshift in D bands and downshift in G bands observed within DC-S compared to DC suggests the characteristic of *n*-type doping of DC-S, which can effectively improve the conductivity of DC-S.[39] The electronic conductivity of DC-S and DC is calculated to be 43.2 and 3.91 mS $m^{-1}$ (Figure S2), respectively, confirming a great enhancement of electronic conductivity after sulfur doping. The FTIR adsorption bands (Figure 2d) of DC-S at 1385, 694 $cm^{-1}$ and 881 $cm^{-1}$ are ascribed to stretching vibrations of C-S and S-S bonds,[37,38] and the band at 1131 $cm^{-1}$ is stretching vibration of S-O bonds,[40] which are consistent with the XPS and Raman results. Besides, the 1672 and 1572 $cm^{-1}$ bands are assigned to breathing vibration of C=O and C=C, showing that NTCDA is totally pyrolyzed to form the structure of condensed aromatics rings with functional groups on the surface.[41]

Nitrogen adsorption-desorption isotherm analysis was further characterized to evaluate the surface area and pore structure of as-obtained products. As given in Figure S3, the Brunauer-Emmett-Teller (BET) measurement suggests a mesoporous structure of the DC-S particle, as evidenced by the nitrogen adsorption/desorption isotherms of IV type. Based on the BET analysis, the specific surface area of the DC-S is calculated to be 117.3 $m^2 g^{-1}$, much higher than that of DC (14.8 $m^2 g^{-1}$).

The electrochemical properties of the DC and DC-S electrodes were characterized by cyclic voltammetry (CV) and galvanostatic charge-discharge cycling. Figure 3a and 3b show the initial four CV curves of the DC and DC-S electrodes in the range of 0.01-3 V at a scan rate of 0.1 mV $s^{-1}$, respectively. For the DC electrode, a large irreversible cathodic peak is observed at about 0.8 V in the first cycle and disappears in the subsequent cycles, which may be related to the irreversible reaction of Na with functional groups and the formation of solid-electrolyte interphase (SEI). Similar phenomenon was reported previously in Li and Na storage in the carbonaceous materials. The weak cathodic peak near 1.3 V can be attributed to the

reactions of Na with functional groups at the carbon surface, while the redox peaks below 0.7 V are related to $Na^+$ insertion/extraction into/from carbon layers, respectively. Compared to the DC electrode, the CV curves for the DC-S electrode (Figure 3b) exhibit two extra distinguishing redox couples located at 1.75/2.2 V and 1.15/1.8 V, which can be attributed to a stepped redox reactions between S and Na, similar to that reported in the room-temperature Na-S batteries.[32,33] It indicates that the covalently bonded S is electrochemically active and can additionally accommodates Na, thus enhancing the reversible capacity.

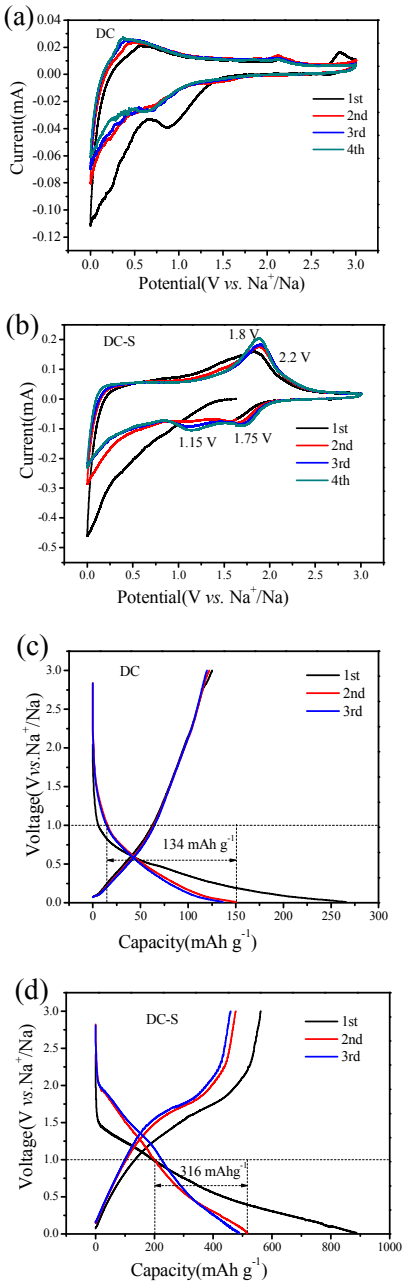


***Figure 3.*** The CV curves of (a) DC, and (b) DC-S electrode in a voltage range of 3.0-0.01 V at a scan rate of 0.1 mV $s^{-1}$. The charge-discharge profiles of (c) DC, and (d) DC-S electrode at the current density density of 0.02 A $g^{-1}$.

Figure 3c and 3d display the charge and discharge profiles of the DC and DC-S electrode. The DC electrode releases an initial discharge and charge capacity of 267 and 126 mAh $g^{-1}$ at a current density of 0.02 A $g^{-1}$ (Figure 3c), which is analogous to previous reported Na storage performance in disordered carbons.[24,29,31] Interestingly, the DC-S electrode delivers an extremely high initial discharge and charge capacity of 887 and 561 mAh $g^{-1}$, respectively, demonstrating a great reversible capacity enhancement of four times higher than that of the DC anode. In addition, the initial coulombic efficiency of the DC-S electrode (~ 63.2%) is much higher than the DC electrode (47.3%), which is related to the low oxygen content of DC-S(9.2 wt% for DC-S, 18.53 wt% for DC, Table S1) since oxygen functional groups generally cause much irreversible reactions during the initial cycle. [39] High reversible capacity of ca. 500 mAh $g^{-1}$ is stably maintained in the following cycles for the DC-S and the voltage profile exhibits mainly two sloped regions: a high voltage region (1.0~2.0 V) and a low voltage region (below 1.0 V). The first region is related to the reaction between the covalently bonded S and Na, which agrees well with the CV results (Figure 3b). The second region is very similar to the voltage profiles of the DC (Figure 3c) and is ascribed to the reversible Na adsorption/insertion on/between the carbon layers, which contributes a reversible capacity of about 316 mAh $g^{-1}$ ($2^{nd}$ cycle, Figure 3d). This value is obviously higher than that delivered by the DC from the same voltage region (316 mAh $g^{-1}$ vs. 134 mAh $g^{-1}$), indicating that the electrochemical activity of the carbon materials is greatly enhanced by sulfur doping. It is worth noted that, significant capacity enhancement are obtained in both regions for DC-S, which demonstrates that the sulfurization process not only provides additional Na storage sites by high S heteroatom loading, but also increases the electrochemical activity of the carbon materials by increasing the surface area, improving the conductivity and enlarging the interlayer spacing of $d_{002}$, resulting in the great enhancement of reversible capacity.

To gain insight into the additional Na storage mechanism of the atomic bonded S, high resolution XPS of S2p characterizations were performed on the fully discharged and charged DC-S electrode. As shown in Figure 4, at the fully discharged to 0.01 V (Figure 4a), the binding energy for the S2p3/2 and S2p1/2 peak significantly shifts to a lower value of 160.9 and 162.5 eV compared to the as-prepared DC-S (Figure 2b), suggesting the low valence state of S

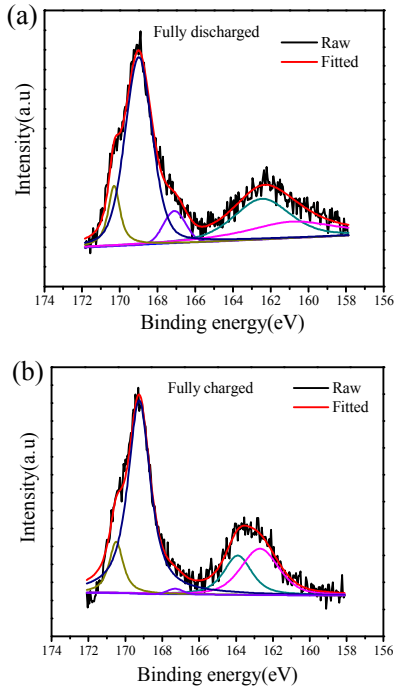


***Figure 4.*** High resolution XPS of S2p of DC-S at (a) fully discharged and (b) fully charged state

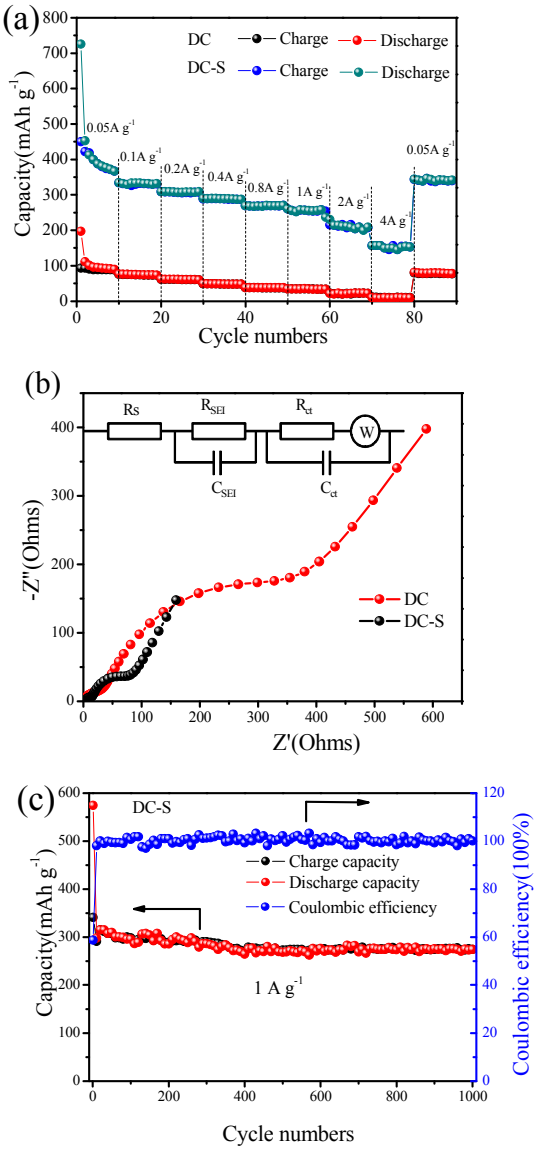


***Figure 5.*** (a) Rate capability of the DC-S and DC electrodes at various current density from 0.05 to 4 A $g^{-1}$. (b) Nyquist plots of DC-S and DC after initial cycle. Inserted is the equivalent circuit. (c) Cycling performance and coulombic efficiency of the DC-S electrode at current density of 1 A $g^{-1}$

due to the strong interaction of Na and S. When fully charged to 3.0 V (Figure 4b), the S2p3/2 and S2p1/2 peaks shift positively to 162.6 and 163.9 eV (lower than the pristine 163.7 and 164.8 eV), respectively, indicating the partial oxidative of S. Besides, three extra high binding energy peaks at 167.1, 169.1 and 170.4 eV can be also observed at fully discharged and charged state, which may be related to SEI film during cycling. [43]The changes of binding energy of S2p reveal that the electrochemical reaction of S and Na involves the C-$S_x$-C($x$=1-2) bond cleavage and rearrangement of sulfur atoms, which can be further evidenced by Raman shift. As shown in the Raman spectra in Figure S4, when fully discharged to 0.01 V, the peaks at ~360 $cm^{-1}$(C-S bond) and ~485 $cm^{-1}$(S-S bond) are vanished and then reappeared at the fully charged state (3.0 V), confirming the cleavage and reconstruction of the C-$S_x$-C ($x$=1-2)bonds.

In addition to the dramatically enhanced capacity, the DC-S electrode also exhibits superior rate capability and long cycling stability. Figure 5a presents the capacity of the DC-S electrode at different current density from 0.05 to 4 A $g^{-1}$.The electrode delivers a reversible capacity of 360, 333, 320, 302, 288 and 275 and 211 mAh $g^{-1}$ at the current density of 0.05, 0.1, 0.2, 0.4, 0.8, 1 and 2 A $g^{-1}$, respectively. Even at a very high current density of 4 A $g^{-1}$, a capacity of 158 mAh $g^{-1}$ is still delivered. In comparison, the DC electrode shows much poor rate performance, and the reversible capacity is rapidly declined to less than 20 mAh $g^{-1}$with the current density increased to 4 A $g^{-1}$. Furthermore, after 80 cycles at various high rates, the DC-S electrode regains a reversible capacity of 355 mAh $g^{-1}$ when the current density returns to 0.05 A $g^{-1}$, demonstrating an outstanding high rate cyclability. Apparently, the excellent rate capability of the DC-S is benefited from the unique coral-like structure with an interconnected 3D framework, which is

propitious to the fast charge transfer and ion diffusion by reducing the diffusion distance. Impedance spectrospecopy analysis (Figure 5b) shows that the DC-S electrode exhibits a much lower SEI film resistance ($R_{SEI}$, 14.3 Ω) and charge transfer resistance ($R_{ct}$, 52.4 Ω) than those of DC electrode (35.8 Ω and 284.3 Ω) based on the equivalent circuit simulation, respectively, indicating that the DC-S electrode has a thinner SEI film favoring rapid $Na^+$ insertion/extraction and facile charge transfer at the electrode/electrolyte interface. Moreover, sulfur doping favors the DC-S with enhanced electronic conductivity, which may be interpreted as the C-$S_x$-C($x$ =1-2) bond in/between the carbon layers providing an alternative route for the electron transfer and guarantees the continuous and rapid electron transport.[44]

The cycling performance of DC-S was further evaluated at a high current density of 1 A $g^{-1}$ shown in Figure 5c. A reversible capacity of 271 mAh $g^{-1}$ is obtained even after 1000 cycles with capacity retention of 85.9% based on capacity of the second cycle, corresponding to a capacity decay of 0.016% per cycle. The coulombic efficiency approaches 100% after several cycles, indicating a stable reversibility. It is further confirmed by the SEM image of the DC-S electrode before and after 1000 cycles at 1 A $g^{-1}$ shown in Figure S5. There is no obvious morphology change after long cycling at high rate, demonstrating a robust structure of the DC-S.

Such a high sodium storage capacity with excellent cycling stability (>1000 cycles) has seldom been achieved in previous reports on carbon-based anode materials for SIBs. The superior electrochemical performance of the sulfur-doped carbon can be mainly attributed to the synergistic effect of well-developed 3D porous structure and the high sulfur doping. First, the unique coral-like structure with an interconnected 3D framework provides the DC-S with more active sites for Na storage and facilitates the transfer of $Na^+$ and electrons in the electrode. Moreover, a large interlayer spacing in the DC-S guarantees a more favorable insertion and extraction of $Na^+$, thus enhance the Na storage capability. Second, the sulfur atoms covalently bonded to the pyrolytic carbon are electrochemically active and can be the accommodation sites for Na, leading to high reversible capacity. Moreover, the electronic conductivity of disorder carbon is significantly improved after sulfur doping, resulting in remarkably enhanced electrochemical performance.

In summary, we have successfully synthesized a high performance sulfur-doped carbon anode for SIBs, with a convenient, economical, and scalable method. Benefiting from high sulfur doping level and the unique 3D coral-like structure, the as-prepared sulfur-doped carbon exhibits high reversible capacity (516 mAh $g^{-1}$ at 0.02 A $g^{-1}$), excellent rate performance (158 mAh $g^{-1}$ at 4 A $g^{-1}$) and superior cycling performance (271 mAh $g^{-1}$ at a current density of 1A $g^{-1}$ after 1000 cycles with a capacity retention of 85.9%). This work may provide a new strategy to develop high performance carbon-based anodes for low cost sodium ion batteries and other electrochemical energy storage applications.

## Acknowledgements

This work was supported by the Natural Science Foundation of China (Grant 51307069), 973 Program (2015CB258400) and the National Thousand Talents Program of China.

## Notes and references

1 D. Kundu, E. Talaie, V. Duffort, and L. F. Nazar, *Angew. Chem. Int. Ed.*, 2015, **54**, 3431-3448.

2 N. Yabuuchi, K. Kubota, M. Dahbi, S. Komaba, *Chem. Rev.*, 2014, **114**, 11636-11682.

3 S. W. Kim, D. H. Seo, X. H. Ma, G. Ceder, K. Kang, *Adv. Energy Mater*., 2012, **2**, 710-721.

4 M. D. Slater, D. Kim, E. Lee, C. S. Johnson, *Adv. Funct. Mater*., 2013, **23**, 947-958.

5 B. Dunn, H. Kamath , J. M. Tarascon, *Science*, 2011, **334**, 928-935.

6 H. N. He, X. G. Zeng, H. Y. Wang, N. Chen, D. Sun, Y. G. Tang, X. B. Huang, and Y. F. Pan, *J.Electrochem. Soc.*, 2015, **162**, A39-A43.

7 M. Dahbi, N. Yabuuchi, K. Kubota, K. Tokiwa ,S. Komaba, *Phys. Chem. Chem. Phys.*, 2014, **16**, 15007-15028.

8 H. S. Hou, M. J. Jing, Y. C. Yang, Y. Zhang, W. X. Song, X. M. Yang, J. Chen, Q. Y. Chen, X. B. Ji, *J. Power Sources*, 2015, **284**, 227-235.

9 Y. C. Liu, N. Zhang, L. F. Jiao, Z. L. Tao, and J. Chen, *Adv. Funct. Mater.*, 2015, **25**, 214-220.

10 Y. Liu, Y. Xu, Y. Zhu, J. N. Culver, C. A. Lundgren, K. Xu, C. Wang, *ACS Nano*, 2013, **7**, 3627-3634.

11 J. F. Qian, Y. Chen, L. Wu, Y. L. Cao, X. P. Ai, H. X. Yang, *Chem. Commun.*, 2012, **48** , 7070-7072.

12 A. Rudola, K. Saravanan, C. W. Mason, P. Balaya, *J. Mater. Chem. A*, 2013, **1**, 2653-2662.

13 R. Alcántara, F. J. Fernández Madrigal, P.Lavela, J. L. Tirado, J. M. Jiménez Mateos, C. Gómez de Salazar, R. Stoyanova, E. Zhecheva, *Carbon*, 2000, **38**, 1031-1041.

14 R. Alcántara, P. Lavela, G. F. Ortiz, J. L. Tirado, *Electrochem. Solid-State Lett.*, 2005, **8**, 222-225.

15 P. Thomas, D. Billaud, *Electrochim. Acta*, 2000, **46**, 39-47.

16 R. Alcántara, J. M. Jiménez Mateos, P. Lavela, J. L. Tirado, *Electrochem. Commun.*, 2001, **3**, 639-642.

17 D. A. Stevens, J. R. Dahn, *J. Electrochem. Soc.*, 2000, **147**, 1271-1273.

18 K. L. Zhang, X. N. Li, J. W. Liang, Y. C. Zhu, L. Hu, Q. S. Cheng, C. Guo, N. Lin, Y. T. Qian, *Electrochim. Acta*, 2015,**155**, 174-182.



 

19 Y. Kado, Y. Soneda, and N. Yoshizawa, *ECS Electrochem. Lett.*, 2015, **4**, A22-A23.

20 Y. Bai, Z. Wang, C. Wu, R. Xu, F. Wu, Y. C. Liu, H. Li, Y. Li, J. Lu, and K. Amine, *ACS Appl. Mater. Interfaces*, 2015, **7**, 5598-5604.

21 J. T. Xu, M. Wang, N. P. Wickramaratne, M. Jaroniec , S. X. Dou, and L. M. Dai, *Adv. Mater.*, 2015, **27**, 2042-2048.

22 J. Ding, H. Wang, Z. Li, A. Kohandehghan, K. Cui, Z. Xu, B. Zahiri, X. Tan, E. M. Lotfabad, B. C. Olsen, D. Mitlin, *ACS Nano*, 2013, **7**, 11004-11015.

23 E. M. Lotfabad, J. Ding, K. Cui, A. Kohandehghan, W. P. Kalisvaart, M. Hazelton, and D. Mitlin. *ACS Nano*, 2014, **8**, 7115-7129.

24 K. Tang, L. J. Fu, R. J. White, L. H. Yu, M. M. Titirici, M. Antonietti, J. Maier, *Adv. Energy Mater.*, 2012, **2**, 873-877.

25 Y. L. Cao, L. F. Xiao, M. L. Sushko, W. Wang, B. Schwenzer, J. Xiao, Z. M. Nie , L. V. Saraf, Z. G Yang, J. Liu, *Nano Lett.*, 2012, **12**, 3783-3787.

26 W. H. Li, L. C. Zeng, Z. Z. Yang, L. Gu, J. Q. Wang, X. W. Liu, J. X. Cheng, Y. Yu, *Nanoscale*, 2014, **6**, 693-698.

27 Y. X. Wang, S. L. Chou, H. K. Liu, S. X. Dou, *Carbon*, 2013, **57**, 202-208.

28 Y. Yan, Y. X. Yin, Y. G. Guo, L. J. Wan, *Adv. Energy Mater.*, 2014, **4**, 1301584.

29 Z. H. Wang, L. Qie, L. X. Yuan, W. X. Zhang, X. L. Hu, Y. H. Huang, *Carbon*, 2013, **55**, 328-334.

30 H. G. Wang, Z. Wu, F. L. Meng, D. L. Ma, X. L. Huang, L. M. Wang, X. B. Zhang, *ChemSusChem.*, 2013, **6**, 56-60.

31 L. J. Fu, K. Tang, K. P. Song, P. A. V. Aken, Y. Yu, J. Maier, *Nanoscale*, 2014, **6**, 1384-1389.

32 T. H. Hwang, D. S. Jung, J. S. Kim, B. G. Kim, J. W. Choi, *Nano Lett.*, 2013, **13**, 4532-4538.

33 S. Xin, Y. X. Yin, Y. G. Guo, L. J. Wan, *Adv. Mater.*, 2014, **26**, 1261-1265.

34 Y. Yan, Y. X Yin, S. Xin, Y. G. Guo, L. J. Wan, *Chem. Commun.*, 2012, **48**, 10663-10665.

35 W. W. Gao, X. Feng, T. Y. Zhang, H. Zhang, J. Li, and W. B. Song, *ACS Appl. Mater. Interfaces*, 2014, **6**, 19109-19117.

36 X. L. Ma, G. Q. Ning, Y. F. Kan, Y. M. Ma, C. L. Qi, B. Chen, Y. F. Li, X. Y. Lan, J. S. Gao, *Electrochim. Acta*, 2014, **150**, 108-113.

37 P. Piaggio, C. Cuniberti, G. Dellepiane, E. Campani, G. Gorini, G. Masetti, M. Novi, G. Petrillo, *Spectrochim Acta*,1989, **45**,347-356.

38 X. G. Yu, J. Y. Xie, J. Yang, H. J. Huang, K. Wang, Z. S. Wen, *J. Electroanal. Chem.*, 2004, **573**,121-128.

39 G. Q. Ning, X. L. Ma, X. Zhu, Y. M. Cao, Y. Z. Sun, C. L. Qi, Z. J. Fan, Y. F. Li, X. Zhang, X.Y. Lan, and J. S. Gao, *ACS Appl. Mater. Interfaces*, 2014, **6**, 15950-15958.

40 L. Afanador, S. Ortega, R. Gómez, M. E. Niño-Gómez, *Fuel*, 2012, **100**, 43-47.

41 M. Hara, A. Satoh, N. Takami, T. Ohsaki, *J. Phys. Chem.*, 1995, **99**, 16338-16343.

42 Y. S.Yun, V. D. Le, H. Kim, S.J. Chang, S. J.Baek, S.J. Park, B. H. Kim, Y. H. Kim, K. Kang, H. J. Jin, *J. Power Sources*, 2014, **262**, 79-85.

43 X. L. Wang, G. Li, F. M. Hassan, J. D. Li, X. Y. Fan, R. Batmaz, X. C. Xiao, Z. W. Chen, *Nano Energy*, 2015, **15**, 746-754.

44 X. Y. Han, C. X. Chang, L. J. Yuan, T. L. Sun, J. T. Sun, *Adv. Mater.*, 2007, **19**, 1616-1621.

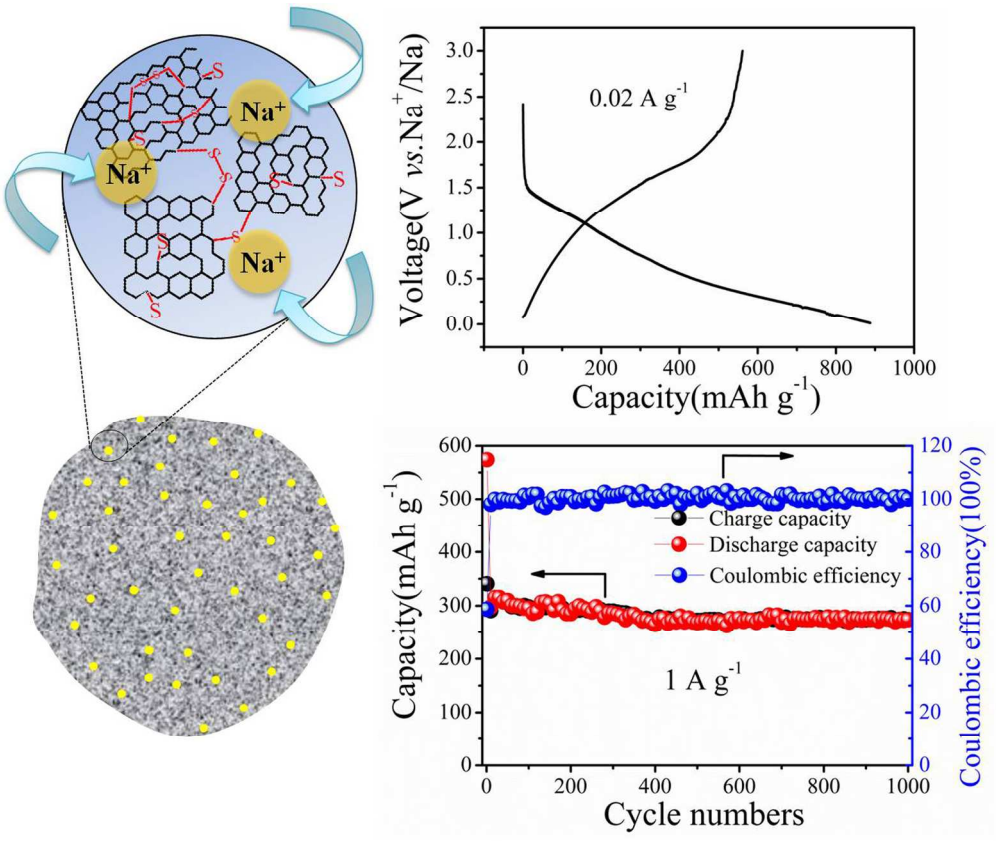


Sulfur-doped disordered carbon exhibits high capacity and excellent cyclability as anode for sodium ion batteries.
187x157mm (300 x 300 DPI)